Cement & Concrete Composites 32 (2010) 497–507

Contents lists available at ScienceDirect

Cement & Concrete Composites

journal homepage: www.elsevier.com/locate/cemconcomp

The ternary system Portland cement–calcium sulphoaluminate clinker–anhydrite: Hydration mechanism and mortar properties

Laure Pelletier *, Frank Winnefeld, Barbara Lothenbach

Empa, Laboratory for Concrete/Construction Chemistry, Überlandstrasse 129, 8600 Dübendorf, Switzerland

ARTICLE INFO

Article history:
Received 9 November 2009
Received in revised form 25 March 2010
Accepted 29 March 2010
Available online 3 April 2010

Keywords:
Ordinary Portland cement
Calcium sulphoaluminate cement
Calcium sulphate
Hydration
Mortar

ABSTRACT

Binders composed of ordinary Portland cement (OPC), calcium sulphoaluminate clinker (CSA) and anhydrite ($C\overline{S}$) were examined in order to study the impact of variations of the OPC:CSA:$C\overline{S}$ ratio on the hydration process and related mortar properties. A first sample series had various anhydrite contents and fixed OPC to CSA ratio, and a second various OPC contents and fixed CSA to $C\overline{S}$ ratio. Experiments made on pastes and thermodynamic modelling showed that the phase assemblage formed during the hydration of the binders was not very sensitive to changes in modal composition, while the ettringite to monosulphoaluminate volume ratio was influenced. All mixes started to hydrate with the formation of ettringite during a reaction involving $C_4A_3\overline{S}$ and calcium sulphate. This generated high early strength. Until about 7 d, mainly the CSA clinker reacted, and 15–20% of the dry binder was converted to ettringite. From about 7 d on, the OPC clinker phase alite reacted significantly, strätlingite, C–S–H and monosulphoaluminate formed, while the ettringite content decreased. According to the laboratory experiments, the CSA clinker was mainly responsible for the early mechanical properties, while OPC played an important role at later ages.

1. Introduction

The hydration processes of ordinary Portland cement (OPC) and of calcium sulphoaluminate cement (CSA) are very well documented. The OPC clinker is mainly composed of four phases, two calcium silicates C_3S and C_2S, one calcium aluminate C_3A, and ferrite C_4AF, to which calcium sulphate is added to control setting. C_3S and C_3A mainly contribute to the early hydration, while C_2S hydrates slower and plays a role for the late properties of the cement [1] (cement notation will be used in the text with A:Al_2O_3, C:CaO, $\overline{C}$:CO_2, F:Fe_2O_3, H:H_2O, M:MgO, S:SiO_2, $\overline{S}$:SO_3). Within the first minutes of hydration, ettringite ($C_3A{\cdot}3C\overline{S}{\cdot}H_{32}$, AFt) forms due to the reaction of C_3A with the added calcium sulphate. After some hours, C_3S begins to hydrate and generates C–S–H, while more AFt is produced via the reaction of C_3A [2,3]. Portlandite (CH) forms within the first hours. After some days, when all the added calcium sulphate is consumed, monocarbonate ($C_3A{\cdot}C\overline{C}{\cdot}H_{11}$) forms if calcite is present in the cement. If calcite is low or absent, hemicarbonate ($C_3A{\cdot}C\overline{C}_{0.5}{\cdot}H_{12}$) and/or monosulphoaluminate ($C_3A{\cdot}C\overline{S}{\cdot}H_{12}$, AFm) can form [4].

There are three main types of CSA cement used for different purposes. They all have the same main constituent, ye'elimite ($C_4A_3\overline{S}$), a calcium sulphoaluminate phase, but variable accessory phases [5]. The first type is dimensionally stable and contains additional C_2S. The two other types expand and have been used as additives to OPC to prevent shrinkage. The second type is richer in aluminium with C_3A, $C_{12}A_7$, CA and an inert phase C_2AS. The third type contains anhydrite or gypsum and free lime. The hydration products depend on the type of CSA cement used, on the amount of calcium sulphate added and on the water to cement ratio [5–7]. The hydration mechanism in the presence of calcium sulphate is well characterized. If calcium sulphate is present, AFt is the first phase to form within the first hours in association with aluminium hydroxide [6], due to the reaction between $C_4A_3\overline{S}$ and calcium sulphate. The beginning of the AFt formation and of the ye'elimite hydration is related to the reactivity of the added calcium sulphate [8–10]. Both are retarded when the reactivity of the calcium sulphate is low. As soon as all of the calcium sulphate has been consumed and in the absence of free lime, monosulphoaluminate ($C_3A{\cdot}C\overline{S}{\cdot}H_{12}$, AFm) can form, together with aluminium hydroxide. In the presence of free lime, a monosulphoaluminate-hydroxy-AFm-solid solution will form in the cement. If C_2S is present, C–S–H and strätlingite (C_2ASH_8) can be formed. Binders based on the rapid formation of AFt can generate expansion, rapid hardening and high early strength. However, mortars based on sulphoaluminate-belite cement blended with OPC (low $C_4A_3\overline{S}$ system) and cured at 60% or 100%RH show lower strength than OPC at 90 d [11,12].

It is well known that the type and quantity of calcium sulphate added to OPC or CSA influence their hydration process, modifying

* Corresponding author. Tel.: +41 44 823 43 11; fax: +41 44 823 40 35.
E-mail address: laure.pelletier@empa.ch (L. Pelletier).

0958-9465/$ - see front matter © 2010 Elsevier Ltd. All rights reserved.
doi:10.1016/j.cemconcomp.2010.03.010

setting time and durability. In OPC, the added calcium sulphate is optimized considering the amount and the reactivity of the C_3A, in order to form AFt during early hydration [13]. In CSA cement, the amount of calcium sulphate does not generally modify the type of hydrates formed, which are AFt and AFm, but mainly the AFt/AFm ratio and the water demand to achieve complete hydration [10,14]. This has an impact on the porosity and on the mechanical strength of the cement. When excess calcium sulphate is present, AFm will not form in the hydrating binder.

Laboratory clinkers composed of $C_4A_3\overline{S}$, $C_5S_2\overline{S}$ and anhydrite ($C\overline{S}$) with a $C\overline{S}/C_4A_3\overline{S}$ mass ratio of 0.5 are assumed to generate AFt during the following reaction: $C_4A_3\overline{S} + 2C\overline{S} + 38H \rightarrow C_3A{\cdot}3C\overline{S}{\cdot}H_{32} + 2AH_3$. If the water to binder ($C_4A_3\overline{S} + C\overline{S}$) ratio related to this reaction is not satisfied (w/binder of 0.78), the mortars stored at 23 °C and 100%RH tend to expand and/or crack, while the same mortars stored in air shrink [15]. Similar mortars containing additional C_3A have high early strength (1 d), and the curing conditions strongly modify the mechanical resistance reached. Samples stored at 23 °C and 100%RH show compressive strength up to 50 MPa, while samples stored under the same conditions and then placed for 21 d at 65%RH show values >100 MPa [16]. Experiments and thermodynamic modelling performed on CSA cements (CSA clinker + Ca-sulphate) showed that these cements have a chemical shrinkage about two times higher than OPC, reaching ~11 cm^3/100 g dry cement after 28 d [7,17].

In ternary binders composed of Portland clinker, synthesized $C_4A_3\overline{S}$ and calcium sulphate, the reactivity of the calcium sulphate is of high importance for the hydration mechanism of the binder [18]. If the calcium sulphate reacts too slowly, the lack of Ca^{2+} and SO_4^{2-} in solution can generate the formation of AFm instead of AFt.

The precise hydration mechanisms of ternary mixes composed of OPC, CSA clinker and calcium sulphate have not been described yet. The objective of the present study is to characterize the latter hydration process and to determine not only if the two types of clinkers react simultaneously or consecutively, but also which clinker is responsible for the early and late mechanical properties. The influence of the calcium sulphate dosage and of the OPC to CSA ratio on the hydration process was studied. Due to the rapid setting (within a few minutes) and for practical applications, citric acid was added as a set retarder to the ternary binders or mortars.

2. Materials and methods

All of the experiments were carried out using an OPC CEM I 42.5 N (according to EN 197-1), a commercial CSA clinker and a technical anhydrite (Table 1), with specific surfaces of 2810, 4770 and 3820 cm^2/g, respectively. The first sample series were tested to check the influence of the calcium sulphate content on the hydration mechanism (studied OPC:CSA:$C\overline{S}$ mass ratios were 8:3:0.5, 8:3:0.75, 8:3:1, 8:3:1.25) keeping OPC/CSA constant. In the second series, the influence of the OPC/CSA ratio (5:3:1, 6:3:1, 7:3:1, 8:3:1) was investigated, keeping CSA/$C\overline{S}$ constant. A citric acid content of 0.27% referred to the total binder (OPC + CSA + anhydrite) was added to all the samples. One mix without citric acid (8:3:1w) was prepared to study the impact of citric acid on the hydration process and to serve as a reference. The chemical composition of the materials was measured by X-ray fluorescence (XRF), and free lime content was determined according to Franke [19]. To determine the content of soluble alkalis in the OPC and in the CSA clinker, 10 g of cement/clinker were stirred in 100 ml of deionised water for 5 min at room temperature. The concentrations of Na^+, K^+ and SO_4^{2-} in solution were measured by ion chromatography. The mineralogical composition of the materials was obtained from X-ray diffraction (XRD)/Rietveld analysis.

All of the experiments were performed at 20 °C and at a w/c = 0.5 by mass. Heat flow curves related to the hydration process were obtained by isothermal calorimetry with a Thermometric TAM Air instrument calibrated at 600 mW, where ~5 g of paste was mixed inside the apparatus. In order to determine the mineralogical composition of the samples, 5 g of each mix was prepared and stored in a sealed container for 5 and 30 min, 2 and 6 h, 1, 7, 28 and 90 d. Prior to XRD and thermogravimetric analysis (TGA/DTG), the pastes were crushed, placed in isopropanol for 30 min and rinsed twice with diethyl ether in order to stop hydration. All samples were ground to a particle size < 63 μm. The XRD experiments were performed with a PANalytical X'Pert Pro MPD diffractometer in a θ–θ-configuration employing Cu Kα radiation. The powdered samples were scanned between 5° and 80° with the X'Celerator detector. The TGA analyses were performed with a Mettler Toledo TGA/SDTA851[e], where ~10 mg of sample was placed in an open vessel under N_2 atmosphere, and investigated at a heating rate of 20 °C/minute up to 980 °C.

Table 1
Chemical analysis and phase composition of the materials used.

	OPC	CSA	$C\overline{S}$	OPC		CSA		$C\overline{S}$	
Chemical analysis (g/100 g)[a]				Normative composition (g/100 g)					
CaO	61.9	36.2	40.3	C_3S[d]	56.1	$C_4A_3\overline{S}$[d]	68.1		
SiO_2	19.6	4.1	0.8	β-C_2S[d]	15.5	C_2AS[d]	14.8		
Al_2O_3	5.1	44.8	0.3	$C_3A^d_{cubic}$	3.5	C_3A[d]	3.4		
Fe_2O_3	2.9	1.3	0.2	$C_3A^d_{orthorhombic}$	1.3	CA[d]	7.8		
MgO	2.3	1.1	0.1	C_4AF[d]	11.5	CA_2[d]	1.2		
K_2O	1.01	0.25	0.04	MgO[d]	1.0	CT[d]	3.6		
Na_2O	0.26	0.07	0.03	$CaCO_3$[d]	4.8	MgO[d]	1.0		
SO_3	3.0	8.9	57.2	$C\overline{S}H_2$[d]	4.0	K_2SO_4[e]	0.018		
P_2O_5	0.20	0.08	0.03	K_2SO_4[e]	1.66	Na_2SO_4[e]	0.003		
TiO_2	0.28	2.19	0.01	Na_2SO_4[e]	0.27	CaO (free)[e]	<0.1		
Mn_2O_3	0.07	0.02	0.01	CaO (free)[e]	0.27				
SrO	0.15	0.12							
Cl	0.032	<0.01		Density (g/cm^3)	3.13	Density (g/cm^3)	2.77	Density (g/cm^3)	2.92
LOI	2.68[b]	0.72[b]	0.56[c]	Blaine (cm^2/g)	2810	Blaine (cm^2/g)	4770	Blaine (cm^2/g)	3820

[a] XRF data uncorrected for loss on ignition (LOI).
[b] 950 °C.
[c] 900 °C.
[d] From Rietveld analysis.
[e] From chemical analysis.

For scanning electron microscopy (SEM), hydration of the samples was stopped (as for XRD), and they were subsequently stored at 40 °C for 2 d before vacuum impregnation with epoxy resin. The microscope was operated at 15 kV for the acquisition of backscattered electron images and EDX semi-quantitative analyses. In order to quantify the main phases and the evolution of the porosity, the image analysis technique described by Ben Haha [20] was used. This method is based on the segmentation of grey levels from backscattered electron images and the pore size investigated is $\geqslant 0.3$ μm.

For strength measurements, mortars were mixed according to the EN 196-1 and 4 cm × 4 cm × 16 cm prisms were produced. They were removed from the mould after 6 h and placed in a humidity chamber at 20 °C and 98% relative humidity until 24 h. Beyond this time, prisms were stored in tap water at 20 °C. Plain OPC mortar was measured as a reference (w/c = 0.5 by mass).

Thermodynamic modelling was used to study the chemical and mineralogical changes associated with the variation of the calcium sulphate or OPC contents in the mixes. It was carried out using the Gibbs free energy minimization program GEMS [21]. GEMS is a broad-purpose geochemical modelling code which computes equilibrium phase assemblage and speciation in a complex chemical system from its total bulk elemental composition. Chemical interactions involving solids, solid solutions, and aqueous electrolytes are considered simultaneously. The speciation of the dissolved species as well as the kind and amount of solids precipitated are calculated [4,22]. The thermodynamic data for aqueous species, gaseous phases as well as solids, were taken from the PSI-GEMS thermodynamic database [23,24]. Cement specific data were taken from Lothenbach et al. [25] and Matschei et al. [26]. A case where 50% of the OPC clinker has reacted was chosen. It approximately corresponds to the hydration of the 8:3:1 ternary binder after 28 d at 20 °C. For the calculations, a w/c of 0.5 was used and was shown to be sufficient for the full hydration of the CSA clinker and of 50% of the OPC.

3. Characterization of the hydration mechanism

3.1. Calorimetry

All samples are characterized by the presence of two peaks within the first 24 h (Fig. 1a–b). In all the binders, the two peaks appear at the same time. The first peak occurs between 20 and 25 min, while the second one begins at approximately 2 h. The first peak is very intense and sharp, while the second peak is less intense and broad. In the binder without citric acid (8:3:1w), the first peak occurs sooner after 5 min and the second one begins at 1.5 h. After 2 d, the binder without citric acid shows two additional broad peaks exhibiting a very low heat flow, while these two peaks did not appear in the other samples during the first 7 d (Fig. 2).

3.2. XRD

The hydrates formed during the hydration process are similar in all the samples with or without citric acid. The amount of calcium sulphate or OPC content only slightly modifies the timing of formation of hydrates or the complete consumption of the anhydrous phases (Table 2). The hydration mechanism can be subdivided into three periods. The first period relates to the early hydration (first 24 h) and is characterized by the dissolution of $C_4A_3\overline{S}$ and of the two calcium sulphates present in the binder ($C\overline{S}$ and $C\overline{S}H_2$ from the OPC). AFt is formed simultaneously (Fig. 3a–b). Its formation is quick and it is present after 5 min. Gypsum is exhausted from the system before anhydrite (Table 2). Secondary gypsum from the hydration of anhydrite was never observed. After some days,

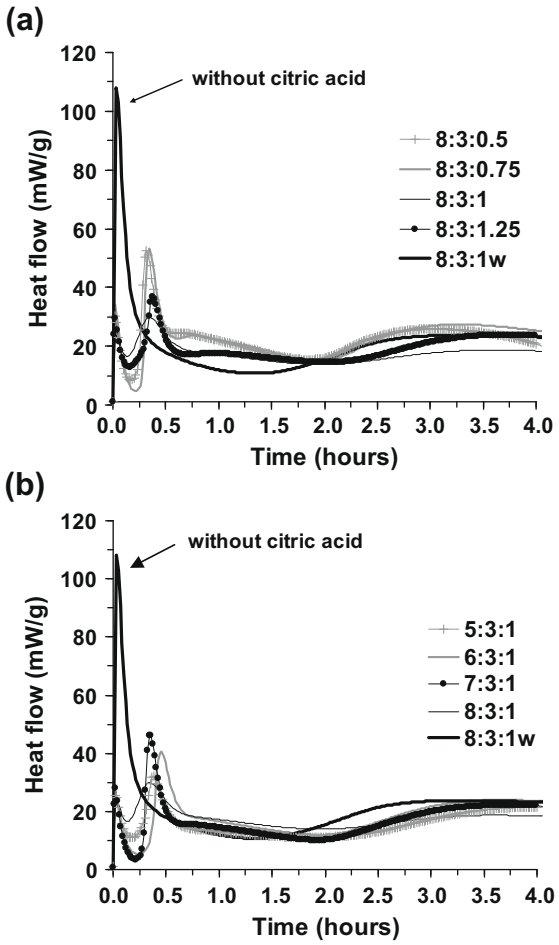

Fig. 1. Heat flow calorimetry on the ternary binders with (a) various calcium sulphate contents and (b) various OPC contents. OPC:CSA:$C\overline{S}$ ratios are given as mass ratios. "w" indicates the absence of the citric acid retarder.

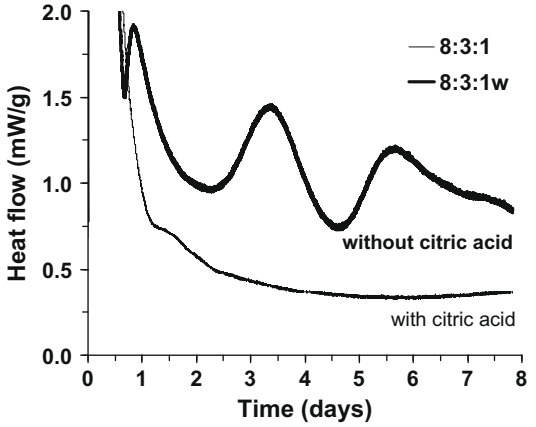

Fig. 2. Heat flow calorimetry on the ternary binders illustrating the hydration process occurring after some days. All samples with citric acid are comparable to 8:3:1 and were omitted. OPC:CSA:$C\overline{S}$ ratios are given as mass ratios. "w" indicates the absence of the citric acid retarder.

all the calcium sulphates have been consumed, and C_4AH_x, strätlingite (C_2ASH_8) and hemicarbonate are formed (Fig. 3b). The third period includes the formation of monosulphoaluminate and monocarbonate. From our results, the second and third periods are distinct in 8:3:1 and 8:3:1w, while they are overlapping in the

Table 2
Hydration kinetics of the studied mixes.

OPC:CSA:$C\bar{S}$ mass ratios	Consumption		Formation							
	$C\bar{S}H_2$	$C\bar{S}$	$C_4A_3\bar{S}$	AFt	AFt max	AFt max[a] (g/100 g)	AFt 90 d[a] (g/100 g)	AH_3[b]	Other I[c]	Other II[d]
8:3:0.5	30 min–2 h	2–6 h	28–90 d	0–5 min	1 d	19	12	30 min–2 h	7 d–28 d[e]	7 d–28 d
8:3:0.75	30 min–2 h	2–6 h	7–28 d	0–5 min	1 d	22	12	30 min–2 h	7 d–28 d	7 d–28 d
8:3:1	30 min–2 h	2–6 h	7–28 d	0–5 min	6 h	18	16	30 min–2 h	7 d–28 d	28 d–90 d
8:3:1.25	30 min–2 h	6 h–1 d	7–28 d	0–5 min	6 h	19	15	30 min–2 h	7 d–28 d	7 d–28 d
6:3:1	30 min–2 h	6 h–1 d	7–28 d	0–5 min	6 h	19	17	30 min–2 h	7 d–28 d	7 d–28 d
7:3:1	30 min–2 h	2–6 h	7–28 d	0–5 min	1 d	19	15	30 min–2 h	7 d–28 d	7 d–28 d
8:3:1w	30 min–2 h	2–6 h	1–7 d	0–5 min	6 h	18	15	30 min–2 h	1 d–7 d	28 d–90 d

The term consumption refers to the disappearance of the XRD signal of $C\bar{S}H_2$, $C\bar{S}$ or $C_4A_3\bar{S}$.
[a] Calculated from TGA analysis.
[b] Deduced from TGA curves.
[c] Includes C_4AH_x, strätlingite, hemicarbonate.
[d] Includes monosulphoaluminate and monocarbonate.
[e] Except for strätlingite 1 d–7 d.

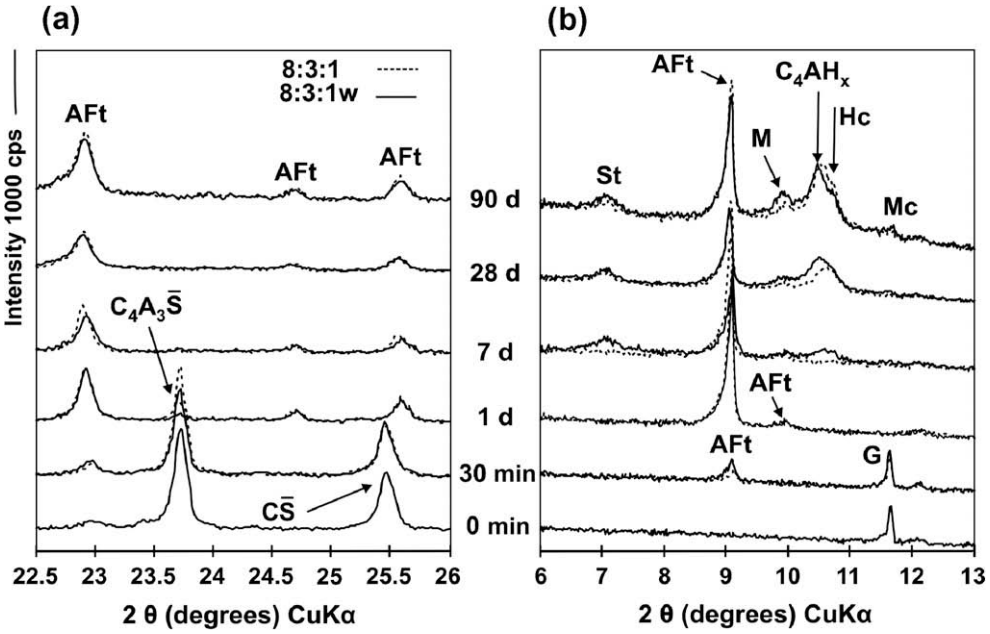

Fig. 3. Variation of XRD diffractograms of 8:3:1w and 8:3:1 with time illustrating (a) ye'elimite and anhydrite consumption and (b) crystallization of the hydrates. AFt = ettringite, $C_4A_3\bar{S}$ = ye'elimite, $C\bar{S}$ = anhydrite, St = strätlingite, C_4AH_x = hydroxy-AFm, M = monosulphoaluminate, G = gypsum, Hc = hemicarbonate and Mc = monocarbonate. OPC:CSA:$C\bar{S}$ ratios are given as mass ratios. "w" indicates the absence of the citric acid retarder.

other mixes (Table 2). This could be due to a lack of sampling between 7 and 28 d. Crystalline aluminium hydroxide (AH_3) was not observed by XRD.

3.3. TGA

The TGA analyses confirmed the mineralogical observations made by XRD. AFt is formed very fast in all the systems and its content is very high after 1 d (Fig. 4). For that reason, the AFt-related peak certainly covers some smaller peaks in the range 50–200 °C, like the ones of strätlingite, hemicarbonate or monocarbonate. It can also partially cover the series of peaks related to monosulphoaluminate and C_4AH_x. The amount of AFt present in the various binders was calculated from the TGA curves in the range 50–110 °C to avoid the main overlaps. According to reference measurement on pure ettringite dried as in the present study, 20 water molecules were associated with AFt. The results are semi-quantitative and presented in Fig. 5. From the TGA curves, the presence of aluminium hydroxide (AH_3) was observed. The derivative curves show a broad and flat signal in the range ~200–300 °C (<0.01%/K) appearing between 30 min and 2 h. This period corresponds to the one of AFt formation. For that reason, the observed broad peak is probably not related to the monosulphate phases, but to AH_3. However, it cannot be excluded that the aluminium hydroxide gel is also linked to some free water molecules, which could lead to an additional water loss around 100 °C during the TGA analysis. The AH_3 is certainly amorphous or micro-crystalline, as it was not observed in any XRD spectrum. At later ages when monosulphoaluminate or C_4AH_x are present in the system, the presence or absence of AH_3 cannot be deduced from the TGA curves because of the overlap of these different signals.

In all the binders containing citric acid, the AFt formation is retarded compared with the binder mixed with water (8:3:1w). However, AFt appears after 5 min in all cases (Table 2). In the two sample series, the amount of AFt is similar in all the mixes at 6 h including the one mixed with water without citric acid (Fig. 5a–b). The series with various calcium sulphate contents can be subdivided into two groups. The first group is characterized by low sulphate contents (8:3:0.5, 8:3:0.75), a maximum AFt content reached at 1 d and a strong decrease in the AFt content after

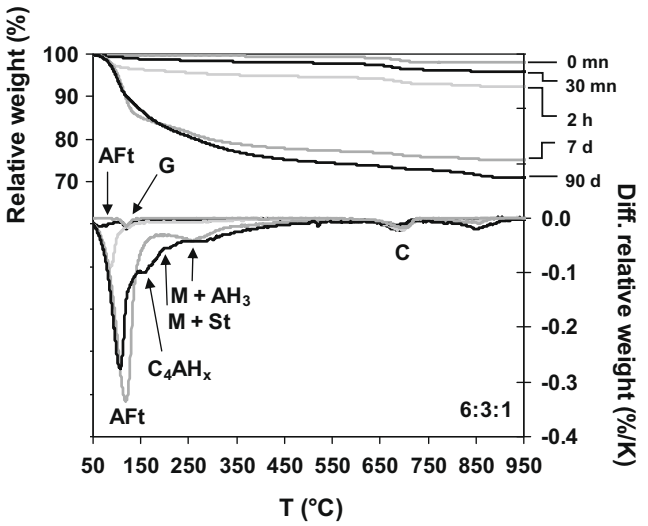

Fig. 4. TGA data of the binder 6:3:1 over time. AFt = ettringite, AH_3 = amorphous or micro-crystalline aluminium hydroxide, C_4AH_x = hydroxy-AFm, M = monosulphoaluminate, St = strätlingite, G = gypsum, C = calcite.

the maximum peak (Fig. 5a). The second group has higher sulphate contents (8:3:1, 8:3:1.25), a maximum AFt content reached after 6 h and a weak decrease in the AFt content after the maximum (Fig. 5a). In the series with increasing OPC content, the mixes also show a maximum AFt content and then a decrease (Fig. 5b). At 2 h, when all the gypsum has been consumed (anhydrite is still present), the OPC-rich samples contain more AFt than the OPC-poor samples.

A main difference between the various binders is related to the AFt to AFm-phase ratio which changes between 7 and 28 d. During this transition, the AFt content seems to decrease, while C_4AH_x and monosulphoaluminate increase (Figs. 3 and 4). This observation is valid for both sample series (variation of calcium sulphate and OPC, respectively).

4. Characterization of the microstructure and chemical composition of the hydrates

4.1. Scanning electron microscopy

The samples 8:3:1 and 6:3:1 were analyzed by SEM to determine the evolution of the microstructure and the mineralogical

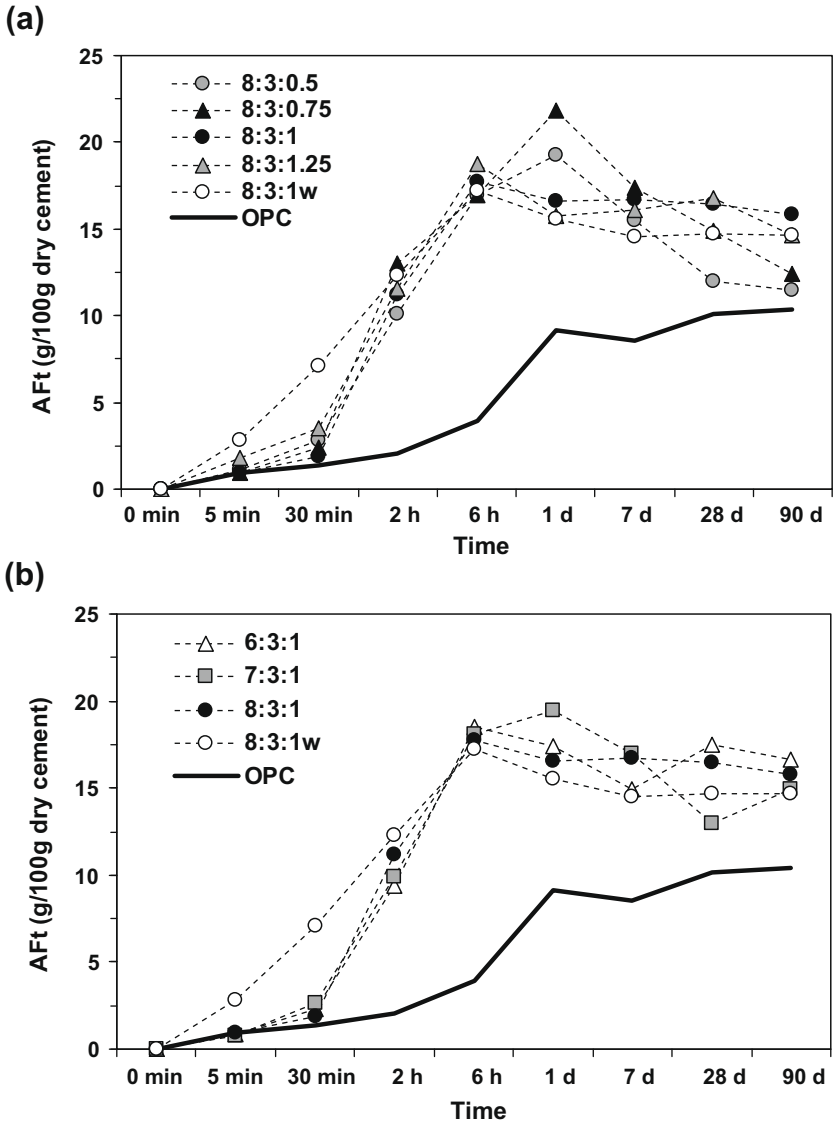

Fig. 5. Amount of AFt as a function of time calculated from the TGA analyses (qualitative) in (a) series with varying calcium sulphate contents and (b) series with various OPC contents. OPC:CSA:C$\overline{S}$ ratios are given as mass ratios. "w" indicates the absence of the citric acid retarder.

composition of their hydrated matrix. The two samples show a similar microstructure and chemical evolution. After 6 h, the CSA clinker grains have already reacted and show irregular rims due to the onset of reaction (Fig. 6a), while the OPC clinker grains appear still intact (Fig. 6e). In both samples, the presence of AH_3 was easily confirmed until 7 d, because it has a much darker grey level than the other hydrates (allowing the estimation of its volume percentage from image analysis). It has extensively formed before 6 h and fills the majority of the pores. Between 6 h and 7 d, CSA clinker is still responsible for the hydration of the binder. Between 7 and 28 d, the OPC clinker begins to react and shows corroded rims, while the CSA clinker grains are nearly fully consumed (Fig. 6d and h). There is also a modification in the grey level intensity of the matrix, which gets lighter indicating a denser microstructure.

The chemical analyses performed in both samples between 7 and 28 d show that at 7 d, the matrix is AFt-dominated and contains additional C_4AH_x and AH_3 (Fig. 7a and c). In sample 8:3:1, many of the 7 d points are aligned along the AFt-monosulphoaluminate line, while this is not the case in 6:3:1. According to this observation, the matrix of 6:3:1 at 7 d is probably poor in monosulphoaluminate compared to 8:3:1. After 28 d, the chemical composition of the matrix mainly lies in the C–S–H–SO_4–AFm–C_2ASH_8 triangle and is then AFm-dominated (Fig. 7a–d). Diagrams illustrating the Ca/Si ratio clearly show that some OPC clinker has reacted between 7 and 28 d (Fig. 7b and d). The composition of the hydrates formed near the OPC clinker grains is close to that of C–S–H.

The image analysis performed on 8:3:1 confirmed the previous observations (Table 3). The hydration process can be subdivided

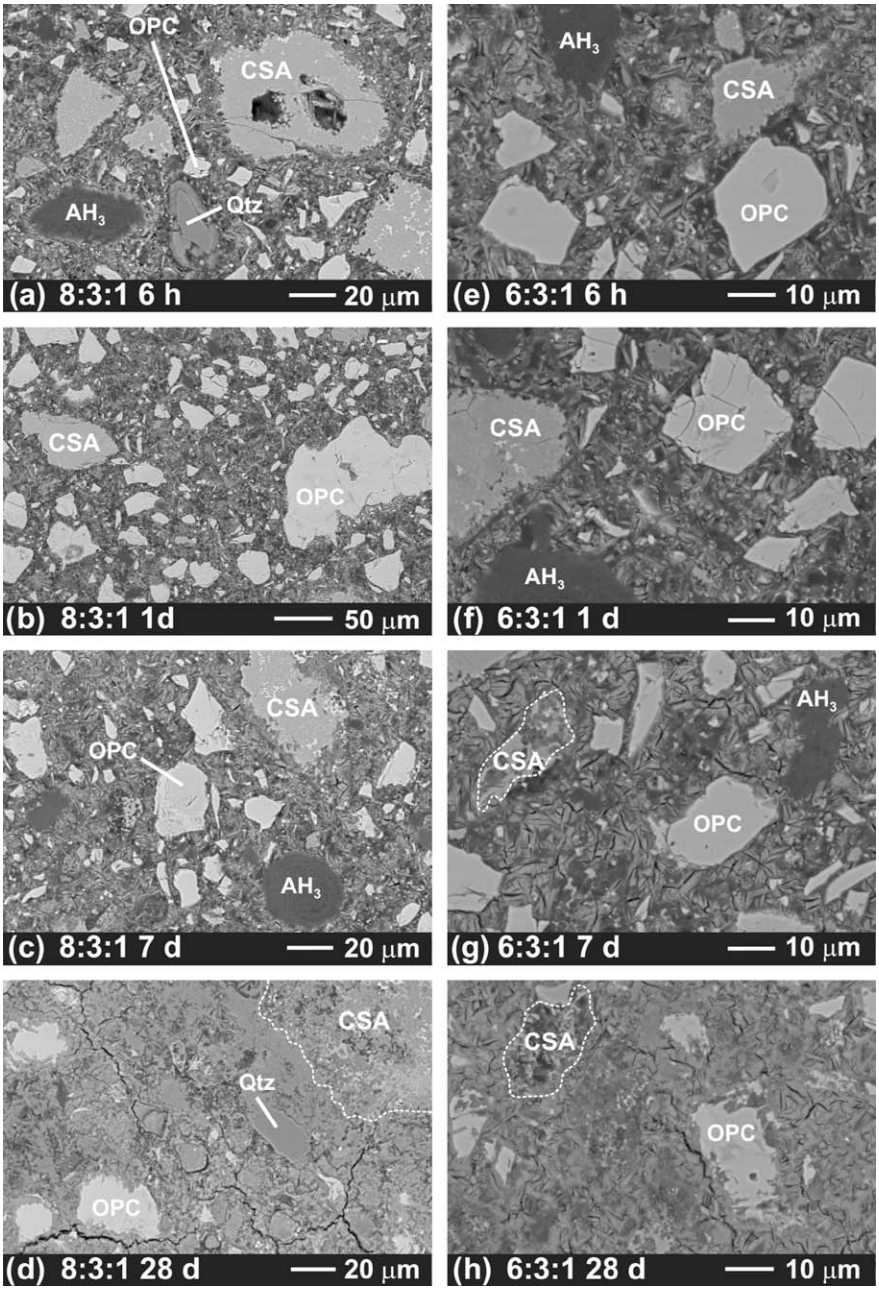

Fig. 6. Backscattered electron images illustrating the textures of (a–d) 8:3:1 and (e–h) 6:3:1 at 6 h, 1, 7 and 28 d. OPC = OPC clinker, CSA = CSA clinker, Qtz = quartz, AH_3 = amorphous or micro-crystalline aluminium hydroxide. OPC:CSA:$C\overline{S}$ ratios are given as mass ratios.

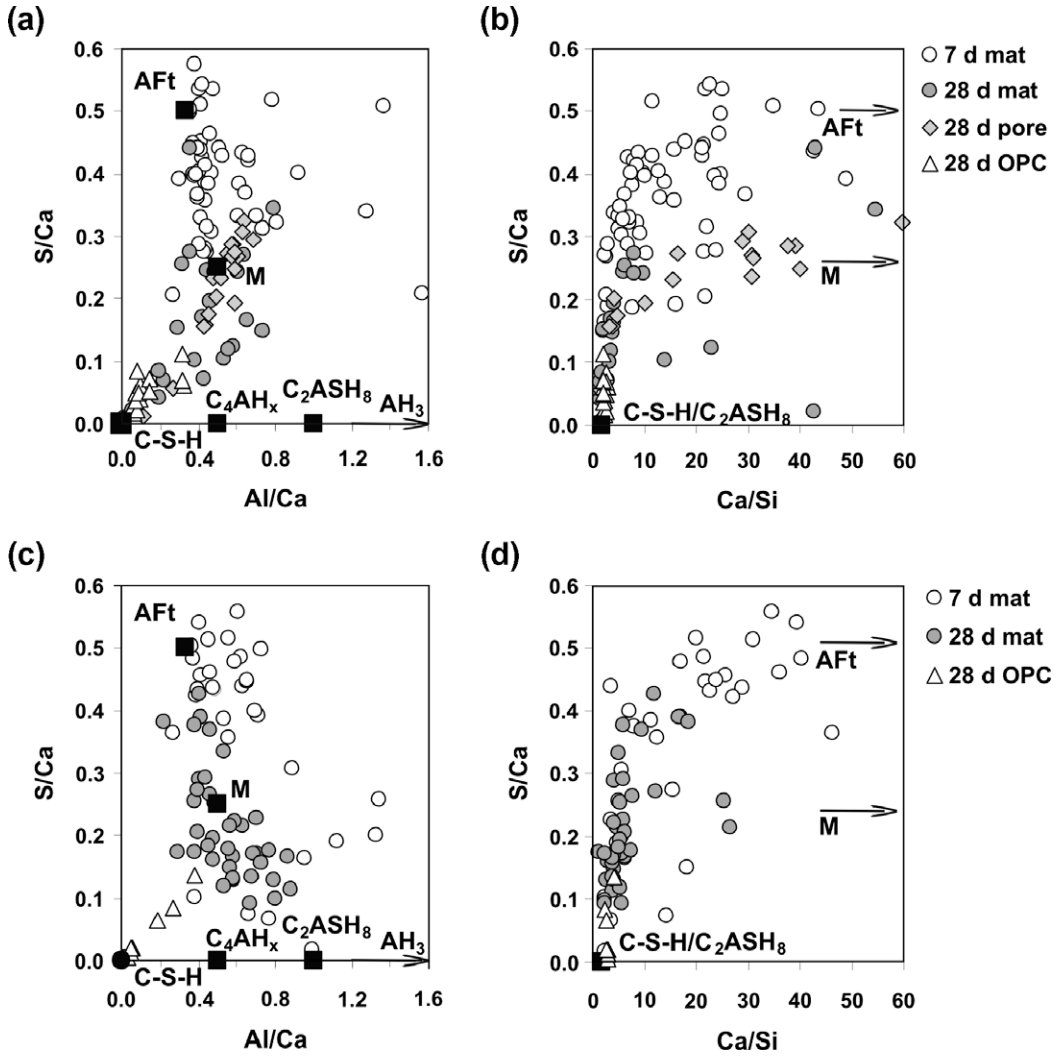

Fig. 7. Semi-quantitative EDX chemical analyses obtained by SEM on hydrates at 7 and 28 d on (a) and (b) sample 8:3:1 and (c) and (d) sample 6:3:1. Results after 6 h and 1 d were omitted because they are similar to the results at 7 d. AFt = ettringite, C_2ASH_8 = strätlingite, C_4AH_x = hydroxy-AFm, M = monosulphoaluminate, AH_3 = amorphous or micro-crystalline aluminium hydroxide, mat = matrix, pore = surface of the air voids, OPC = around OPC clinker grains.

into two periods. During the first period, from mixing to 7 d, the hydration of the binder is mainly dominated by the reaction of the CSA clinker grains with the two calcium sulphates. An important amount of AH_3 is formed with 22 volume% (given as volume as gel-like AH_3 can incorporate more than 1.5 water molecules per Al, giving an overestimated mass fraction), and the porosity is low after 1 d at 8 volume%. The pore size investigated being $\geqslant$0.3 μm, the porosity values refer to capillary pores and do not take the gel pores into account. During the second period, between 7 and 28 d, the reactive CSA clinker phases have been consumed and the OPC clinker content strongly decreases from 22 to 13 volume%. The AH_3 is consumed and the porosity decreases from 4 to 2 volume%. After 28 d, 85 volume% is occupied by hydrates.

The decrease of the porosity observed within the first 7 d corresponds to the one of a CSA clinker with anhydrite at w/c = 0.5 [27]. At this water to cement ratio, the hydration of the CSA clinker with anhydrite is slowed down after 7 d, possibly due to a lack of free water for the further hydration of the clinker [27]. In the ternary system with the same water to cement ratio, about 30 mass% of the initial mixed water is still available after 7 d (calculated from the TGA results and similar for all mixes), allowing the hydration of the OPC and a further decrease of the porosity.

Table 3
Microstructural analysis of 8:3:1 from SEM images.

Volume (%)	0 min	1 d		7 d		28 d	
		Mean	±	Mean	±	Mean	±
CSA clinker	10.9	8	1	7	2	0	0
OPC clinker	25.6	21	4	22	2	13	3
Anhydrite	3.4	0	0	0	0	0	0
AH_3	–	22	2	19	2	–[a]	–[a]
Other hydrates	–	42	2	48	3	85	3
Pores ($\geqslant$0.3 μm)	–	8	1	4	1	2	1

[a] Too small to be quantified separately, included in other hydrates. Volume at 0 min calculated from mass% and density of the materials.

4.2. Mortar properties

4.2.1. Flexural and compressive strength

All the samples could be demoulded after 6 h, because they show good flexural and compressive strengths at that age, 0.2–1.7 MPa and 2–8 MPa, respectively. In the first sample series (keeping OPC/CSA constant) at 7 and 100 d, the higher the calcium sulphate content the higher the compressive strength (Fig. 8a). After 7 d, the samples from the first series show values between 12

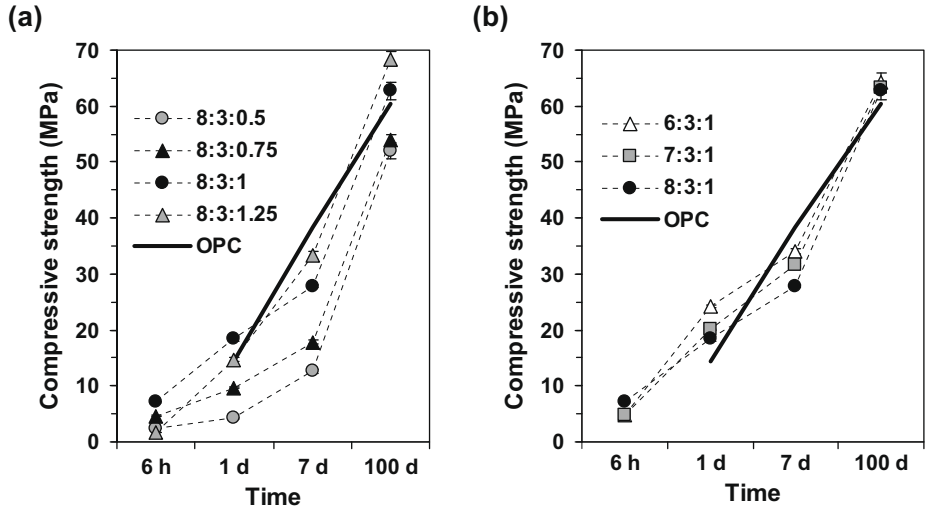

Fig. 8. Compressive strength of the two sample series (a) with various calcium sulphate contents and (b) with various OPC contents. OPC was stored under similar conditions. OPC:CSA:$C\overline{S}$ ratios are given as mass ratios.

and 35 MPa and continue to gain strength until 100 d. In the second sample series (keeping CSA/$C\overline{S}$ constant), the OPC content influences the compressive strength at 1 and 7 d, where the lower the OPC content the higher the strength (Fig. 8b). At 6 h or 100 d, all the samples from the second series show similar values.

4.2.2. Thermodynamic modelling

To visualise the changes in the composition of the hydrate assemblage during the hydration of the OPC-CSA-anhydrite system, the kinetics of dissolution found by XRD for the 8:3:1 mix was used for the modelling (Fig. 9a). The observed progress of dissolution of CSA and OPC was fitted by empirical equations. This empirical description results in a rough estimation of the degree of reaction over time (valid only for the investigated OPC-CSA blend) and enables the calculation of changes in the hydrate assemblage as a function of time.

As described before, $C_4A_3\overline{S}$ initially reacts while the OPC reaction is retarded. The calculations indicate that the reaction of $C_4A_3\overline{S}$ with anhydrite results in the formation of ettringite and AH_3, which is consistent with the hydrates observed within the first days (Figs. 3b and 4). Thermodynamic calculations predict the transformation of anhydrite to gypsum, which was not observed in the experiments as the kinetics of this reaction is relatively slow [28]. For that reason, such formation of gypsum was intentionally prevented in the final model. As the reaction of OPC sets in after approximately a week, the formation of C–S–H (with C/S ratio of approximately 1), monocarbonate, strätlingite and monosulphoaluminate is calculated, which agrees with the experimental observations (Fig. 3). Later the ettringite starts to dissolve, while some monosulphoaluminate is formed.

The modelling of the variation of the anhydrite content shows that it has a low impact on the type of hydrates formed, while it strongly influences the AFt to monosulphoaluminate volume ratio (Fig. 9b). For the anhydrite contents corresponding to our experiments (0.5, 0.75, 1, 1.25), the model additionally predicts the formation of C–S–H, C_4AH_{13} and strätlingite, which are all observed in pastes by XRD and TGA. Some hydrotalcite is also predicted. This phase being poorly crystalline in cement [29], it could be present in the pastes as an XRD-amorphous phase. The model predicts the presence of monocarbonate in the tested mixes, which is not in agreement with the XRD patterns showing the presence of monocarbonate and hemicarbonate. This discrepancy is probably related to slow kinetics of monocarbonate formation. In OPC blended with limestone (4 wt.%), hemicarbonate has been observed as an intermediate phase which was later transformed to monocarbonate [4]. In addition in the calculated mixtures, hemicarbonate is only slightly less stable than monocarbonate. A decrease of the solubility product of hemicarbonate by 0.2 log units (which is well within the inaccuracy of the solubility products used), would lead to the prediction of hemicarbonate and a destabilization of monosulphoaluminate, resulting in the formation of more ettringite and less monocarbonate and a higher total volume.

The modelling of the variation of the OPC content gives a similar phase assemblage (Fig. 9c). The OPC content also influences the AFt to monosulphoaluminate ratio, while it determines the amount of strätlingite which can form in the system. The higher the OPC content the lower the amounts of strätlingite and ettringite formed.

5. Discussion

5.1. Reactions related to the hydration mechanism

The hydration scheme can be subdivided into early hydration where ettringite and AH_3 are the main hydrates to form and late hydration where other hydrates form (C_4AH_x, C_2ASH_8, C–S–H, monosulphoaluminate). From the strong decrease of the $C_4A_3\overline{S}$ and of the gypsum and anhydrite observed in the mixes (Fig. 10), we can conclude that the AFt-forming reaction (1) occurs during the first hydration phase [6].

$$C_4A_3\overline{S} + 2C\overline{S} + 38H \rightarrow C_3A \cdot 3C\overline{S} \cdot H_{32} + 2AH_3 \quad (1)$$

However in the mix with the lowest anhydrite content (8:3:0.5), calculations showed that the calcium sulphate addition is not sufficient to fully react with the $C_4A_3\overline{S}$ via reaction (1) even if gypsum from the OPC is additionally considered as a sulphate source. In this sample, minor quantities of monosulphoaluminate may be produced. Minor quantities of CA or C_3A may participate later in the early hydration when the calcium sulphates are exhausted, leading to the formation of additional monosulphoaluminate. Even if AH_3 was not observed before 2 h by TGA, we assume that reaction (1) is the first and main one to occur because AH_3 was identified after 1 d by SEM (AH_3 is difficult to quantify because it is amorphous or micro-crystalline, and minor quantities may not be detectable by the TGA at early age) and is predicted by the thermodynamic modelling (Fig. 9a). The preferred $C_4A_3\overline{S}$ consumption

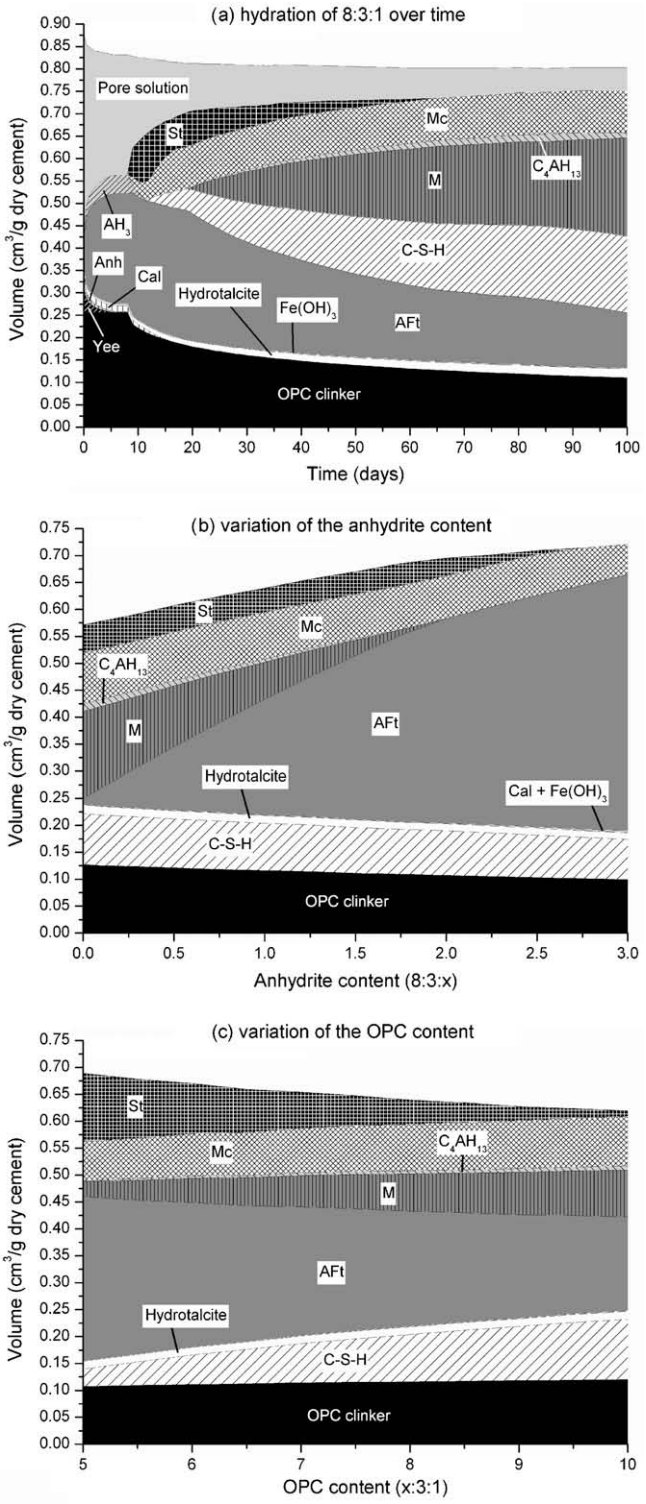

Fig. 9. Modelled hydration of the ternary binder (a) in mix 8:3:1 over time, (b) with the variation of the anhydrite content and (c) with the variation of the OPC content. Volume expressed as cm^3/g dry cement and calculation made with w/c = 0.5 and 20 °C. Variation of the anhydrite or OPC content modelled for 50% of the OPC clinker reacted (equivalent to the hydration of the system after ~28 d). The *x*-axis in (b) and (c) represents OPC:CSA:$C\bar{S}$ as mass ratios. The decrease of the total volume in Fig. 9a corresponds to the calculated chemical shrinkage of the 8:3:1 mix. AFt = ettringite, AH_3 = amorphous or micro-crystalline aluminium hydroxide, Anh = anhydrite, Cal = calcite, M = monosulphoaluminate solid solution with C_4AH_x, Mc = monocarbonate, OPC clinker = unreacted OPC clinker, St = strätlingite, Yee = ye'elimite ($C_4A_3\bar{S}$).

compared to the OPC clinker reaction is well illustrated on the images from the SEM (Fig. 6) and by XRD (Fig. 10). According to these observations, $C_4A_3\bar{S}$ has the highest reactivity in the ternary system.

In a second hydration step the OPC clinker starts to react and C_3S can be consumed via reactions (2), (3) (Fig. 10), producing strätlingite or C–S–H in association with portlandite (CH). Thermodynamic modelling predicts the absence of AH_3 from all the tested mixes at 28 d, which is in agreement with the occurrence of reaction (3) in the pastes. AH_3 can react with portlandite and with the calcite from the OPC to form monocarbonate as in reaction (4).

$$C_3S + AH_3 + 6H \rightarrow C_2ASH_8 + CH \quad (2)$$

$$C_3S + 3.7H \rightarrow CSH_{1.7} + 2CH \quad (3)$$

$$AH_3 + 3CH + C\bar{C} + 5H \rightarrow C_4A\bar{C}H_{11} \quad (4)$$

Simultaneously, C_4AH_x can form from the consumption of the AH_3 produced in reaction (1) or from the C_3A of the OPC (reactions 5 and 6). In any case, CH needs to be present to allow C_4AH_x formation (x = 13 or 19 depending on the relative humidity). Considering the absence of CH during the whole hydration process, we assume that CH could have been produced during reactions (2), (3) and directly consumed in reactions (4)–(6).

$$AH_3 + 4CH + 6H \rightarrow C_4AH_{13} \quad (5)$$

$$C_3A + CH + 12H \rightarrow C_4AH_{13} \quad (6)$$

Finally the monosulphoaluminate forms during reactions (7) and/or (8) consuming some of the pre-existing phases [6]. The occurrence of reaction (7) in 8:3:1 and 6:3:1 was clearly demonstrated during the EDX analyses (Fig. 7) and by the decrease of the ettringite content observed by XRD (Fig. 5). The late consumption of C_3A between 7 and 28 d, illustrated in Fig. 10, is in agreement with reaction (8), the one of CA in reaction (9). These latter reactions have already been observed in ternary systems composed of OPC, calcium aluminate cement and calcium sulphate [30,31].

$$3C_4AH_{13} + 2C_3A \cdot 3C\bar{S} \cdot H_{32} + AH_3 \rightarrow 6C_3A \cdot C\bar{S} \cdot H_{12} + 34H \quad (7)$$

$$C_3A \cdot 3C\bar{S} \cdot H_{32} + 2C_3A + 4H \rightarrow 3C_3A \cdot C\bar{S} \cdot H_{12} \quad (8)$$

$$C_3A \cdot 3C\bar{S} \cdot H_{32} + 6CA + 16H \rightarrow 3C_3A \cdot C\bar{S} \cdot H_{12} + 4AH_3 \quad (9)$$

5.2. Retardation by citric acid addition

Comparing 8:3:1 to 8:3:1w, we can see that the addition of citric acid probably does not strongly modify the $C\bar{S}H_2$ and $C\bar{S}$ dissolution kinetics because these phases disappear within the same time period in both cases (Table 2). $C_4A_3\bar{S}$ consumption and AFt production are slowed down. From the calorimetric curves, it can be seen that the first exothermic peak, which is related to the formation of AFt and AH_3, is delayed by about 20 min (Fig. 1). The broader peaks observable after some days are also delayed in the presence of citric acid (Fig. 2). They are probably related to the onset of the OPC clinker hydration and to the related formation of strätlingite, hemicarbonate or monocarbonate, and/or to monosulphoaluminate formation. From these observations, we can conclude that the retarder has an impact on early and late hydration processes.

In the binder with citric acid, AFt production seems to be subdivided into two periods (Fig. 5). A first period from 0 to 30 min where AFt production is slow and a second one from 30 min to 6 h where AFt production is quicker. In the mix without citric acid, the AFt formation is more linear. According to studies performed on calcium aluminate cements, citrate ions cannot crystallize as

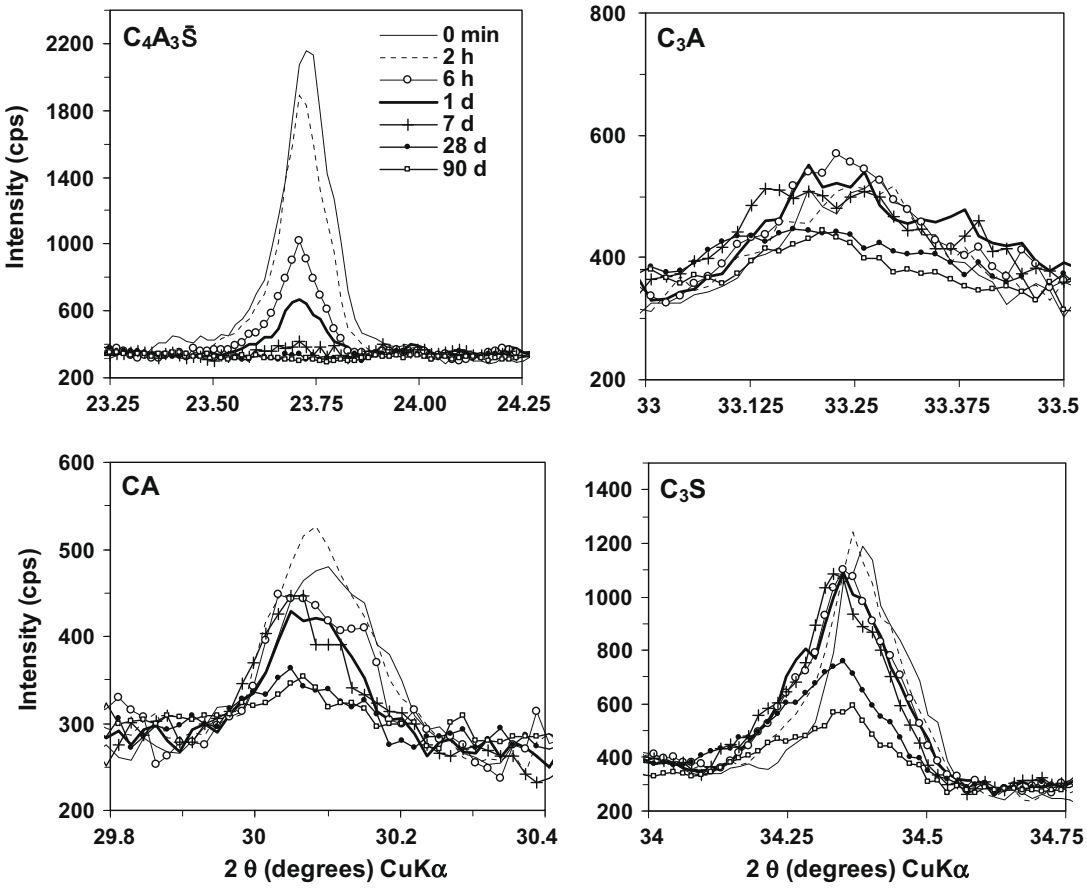

Fig. 10. Variation of selected areas of XRD diffractograms of 8:3:1 illustrating $C_4A_3\bar{S}$ (ye'elimite), CA, C_3A and C_3S consumption with time.

salts, but may be complexed with Ca^{2+} and potentially lower its concentration in the pore solution [32,33]. This could slow down the AFt-formation rate. As the citric acid content in the system was low (0.27% to the binder), this could have influenced the early AFt-formation rate, but as soon as all the citrate ions would have been complexed, the formation rate would have accelerated. On the other hand, the study of Möschner [34] on OPC showed that the complexation of Ca^{2+} is very weak and that citrate slows down hydration by creating a protective layer of sorbed citrate on the clinker grains. It was also demonstrated by Cody [35] that citric acid prevents the nucleation and the crystal growth of ettringite. However, it is beyond the scope of this paper to determine how citric acid retards the hydration of the ternary system.

5.3. Influence of the varying calcium sulphate content

The variation of the calcium sulphate content has little impact on the hydration kinetics of the cement at constant OPC/CSA, and on the phases which form as shown by experimental data and thermodynamic calculations (Figs. 1 and 10a; Table 2). However, it clearly generates two different families in terms of AFt quantity over time and strength development (Figs. 5 and 9a), and it strongly influences the AFt to monosulphoaluminate ratio (Fig. 9b). The first family includes the samples with high calcium sulphate contents (8:3:1 and 8:3:1.25). They show a maximum AFt content after 6 h and a low decrease of this content after the maximum peak. They have the highest compressive strength at 1, 7 and 28 d. The second family includes samples with low calcium sulphate contents (8:3:0.5 and 8:3:0.75). They show a maximum AFt content after 1 d and a strong decrease of this content after the maximum peak. They have the lowest compressive strength at 1, 7 and 28 d.

There is a positive correlation between the AFt to monosulphoaluminate ratio and the compressive strength at later ages (Figs. 8a and 9b). The samples with the higher ratio have the higher compressive strength at a defined age. This is confirmed by the thermodynamic modelling which shows that an increased fraction of anhydrite results in a higher volume of the hydrates and thus to a lower porosity resulting in a higher compressive strength (Figs. 8a and 9b).This is related to the lower volume of monosulphoaluminate compared to AFt. The generation of additional porosity can be roughly estimated from the molar volumes of the reactants and products of the monosulphoaluminate-forming reactions (molar volumes from Ito [36] and Lothenbach [4]). In reaction (7), where the free water produced can be omitted, a volume decrease of about 69 cm^3 per mole of monosulphoaluminate can be calculated. In reactions (8) and (9), where free water can be considered and will generate chemical shrinkage, volume decreases of 10 cm^3 and 86 cm^3 are calculated per mole of monosulphoaluminate produced.

5.4. Influence of the varying OPC content

The variation of the OPC content has little impact on the hydration kinetic of the cement at constant CSA/$C\bar{S}$ ratio, and almost no effect on the phases which form as shown by experimental data and thermodynamic calculations (Figs. 1b and 9c; Table 2). At 1 and 7 d, the higher the OPC content the lower the strength. As OPC clinker participates minimally in the hydration process before 7 d (except for the dissolution of free lime and alkali sulphates), it can be considered mainly as a filler during early hydration and then does not contribute to early strength. The absence of reaction of the OPC clinker during the early hydration is not related to the

addition of the citric acid because the same observations were made without the admixture (8:3:1w).

However, the OPC content slightly influences the AFt to monosulphoaluminate ratio at later ages and the related compressive strength as discussed above (Figs. 7, 8b and 9c). An increased fraction of OPC results in a lower volume of the hydrate phases and thus to a higher porosity resulting in a lower compressive strength. The OPC content can play a role during late hydration because it represents a C_3S and C_3A source for late hydration reactions. C_3S is involved in the strätlingite-forming reaction and C_3A in the monosulphoaluminate-forming reaction. The amount of AH_3 is the limiting factor for the formation of strätlingite. If the OPC content is high, CSA content is low, leading to a lower AFt and AH_3 production. This directly influences the amount of strätlingite which can form (Fig. 9c). According to these observations, we conclude that the OPC content of the binder can strongly influence the late properties of the mortars.

6. Conclusions

Experiments made on pastes and thermodynamic modelling show that the anhydrite content at fixed OPC to CSA ratio or the OPC content at fixed CSA to $C\overline{S}$ ratio do not strongly influence the hydrate assemblage of the ternary binders, while they do determine the AFt to monosulphoaluminate volume ratio. All the ternary binders tested in the present study hydrate very fast and AFt is formed within the first 5 min by the reaction between $C_4A_3\overline{S}$, the main component of the CSA clinker, and the calcium sulphates. The quantity of AFt formed during early hydration can be decreased in the presence of citric acid, but not eliminated (at the studied concentration). Gypsum from the OPC is consumed faster than anhydrite in all mixes. This early hydration reaction generates high early strength with values up to ~8 MPa measured at 6 h. During about 7 d, the CSA clinker is the main one to react and the $C_4A_3\overline{S}$ concentration decreases, achieving a very low value or zero at 28 d. After more than 7 d, C_3S from the OPC begins to hydrate and generates C_2ASH_8 and C–S–H, while AFt reacts with other phases to generate monosulphoaluminate. At 28 d, the hydrates present in all the mixes are the same and include AFt, C_4AH_x, monosulphoaluminate, hemicarbonate, monocarbonate and strätlingite. The rapid formation of ettringite and the related high mechanical resistance observed at early age are promising for the development of fast setting and rapid-hardening materials.

Acknowledgements

The authors would like to thank L. Brunetti, B. Ingold and W. Trindler for their experimental support in the laboratory. Thanks are extended to M. Ben Haha for his help during the data treatment of the secondary electron microscopy, and to the Biomedizin Naturwissenschaft Forschung (BNF) organization from the University of Bern (Switzerland) for its support.

References

[1] Taylor HFW. Cement chemistry. London: Academic Press, Harcourt Brace Jovanovich Publishers; 1990.
[2] Locher FW, Richartz W, Sprung S. Erstarren von Zement. Teil I: Reaktion und Gefügeentwicklung. ZKG Int 1976;10:435–42.
[3] Scrivener KL. The development of microstructure during the hydration of Portland cement. PhD thesis, London, Imperial College of Science and Technology; 1984.
[4] Lothenbach B, Le Saout G, Gallucci E, Scrivener K. Influence of limestone on the hydration of Portland cements. Cem Concr Res 2008;38:848–60.
[5] Lan W, Glasser FP. Hydration of calcium sulphoaluminate cements. Adv Cem Res 1996;8:127–34.
[6] Glasser FP, Zhang L. Calculation of chemical water demand for hydration of calcium sulfoaluminate cement. In: Proceedings 4th international symposium on the cement and concrete, vol. 3; 1998. p. 38–44.
[7] Winnefeld F, Lothenbach B. Hydration of calcium sulfoaluminate cements – experimental findings and thermodynamic modelling. Cem Concr Res in press. doi:10.1016/j.cemconres.2009.08.014.
[8] Sahu S, Havlica J, Tomkova V, Majling J. Hydration behaviour of sulphoaluminate belite cement in the presence of various calcium sulphates. Thermochim Acta 1991;175:45–52.
[9] Winnefeld F, Barlag S. Influence of calcium sulfate and calcium hydroxide on the hydration of calcium sulfoaluminate clinker. ZKG Int 2009;12:42–53.
[10] Winnefeld F, Barlag S. Calorimetric and thermogravimetric study on the influence of calcium sulfate on the hydration of ye'elimite. J Therm Anal Calorim in press. doi:10.1007/s10973-009-0582-6.
[11] Janotka I, Krajči L. An experimental study on the upgrade of sulfoaluminate-belite cement systems by blending with Portland cement. Adv Cem Res 1999;11:35–41.
[12] Palou M, Majling J, Janotka I. The performances of blended cements based on sulfoaluminate belite and Portland cement. In: Grieve G, Owens G, editors. Proceedings 11th ICCC, Durban; 2003. p. 1896–902.
[13] Locher FW, Richartz W, Sprung S. Erstarren von Zement. Teil II: Einfluss des Calciumsulfatzusatzes. ZKG Int 1980;6:271–7.
[14] Glasser FP. Advances in sulfoaluminate cements. In: Proceedings 5th international symposium on the cement and concrete, vol. 1; 2002. p. 14–24.
[15] Beretka J, Marroccoli M, Sherman N, Valenti GL. The influence of C_4A_3s content and w/s ratio on the performance of calcium sulfoaluminate-based cements. Cem Concr Res 1996;26:1673–81.
[16] Sherman N, Beretka J, Santoro L, Valenti GL. Longterm behaviour of hydraulic binders based on calcium sulfoaluminate and calcium sulfosilicate. Cem Concr Res 1995;25:113–26.
[17] Lura P, Winnefeld F, Klemm S. A method for simultaneous measurements of heat of hydration and chemical shrinkage on hardening cement pastes. J Therm Anal Calorim in press. doi:10.1007/s10973-009-0586-2.
[18] Taczuk L, Bayoux JP, Sorrentino F, Capmas A. Understanding of the hydration mechanisms of C_4A_3S–Portland clinker–$CaSO_4$ mixes. In: Mullick AK, editor. Proceedings 9th ICCC, New Delhi: National Council for Cement and Building Materials; 1992. p. 278–84.
[19] Franke A. Bestimmung von Calciumoxid und Calciumhydroxid neben wasserfreiem und wasserhaltigem Calciumsilikat. Z Anorg Allg Chem 1941;247:180–4.
[20] Ben Haha M, Gallucci E, Guidoum A, Scrivener KL. Relation of expansion due to alkali silica reaction to the degree of reaction measured by SEM image analysis. Cem Concr Res 2007;37:1206–14.
[21] Kulik D. GEMS 2.3 software. <http://www.gems.web.psi.ch/download/reposit/selpack.html>, PSI Villigen, Switzerland; 2009.
[22] Lothenbach B, Winnefeld F. Thermodynamic modelling of the hydration of Portland cement. Cem Concr Res 2006;36:209–26.
[23] Hummel W, Berner U, Curti E, Pearson FJ, Thoenen T. Nagra/PSI chemical thermodynamic data base 01/01, Universal Publishers/uPUBLISH.com, USA, also published as Nagra Technical report NTB02 16, Wettingen, Switzerland; 2002.
[24] Thoenen T, Kulik D. Nagra/PSI chemical thermodynamic database 01/01 for the GEM-Selektor (V.2-PSI) geochemical modelling code, PSI Villigen, http://www.gems.web.psi.ch/doc/pdf/TM-44-03-04-web.pdf; 2003.
[25] Lothenbach B, Matschei T, Möschner G, Glasser FP. Thermodynamic modelling of the effect of temperature on the hydration and porosity of Portland cement. Cem Concr Res 2008;38:1–18.
[26] Matschei T, Lothenbach B, Glasser FP. Thermodynamic properties of Portland cement hydrates in the system $CaO–Al_2O_3–SiO_2–CaSO_4–CaCO_3–H_2O$. Cem Concr Res 2007;37:1379–410.
[27] Bernardo G, Telesca A, Valenti GL. A porosimetric study of calcium sulfoaluminate cement pastes cured at early ages. Cem Concr Res 2006;36:1042–7.
[28] Kontrec J, Kralj D, Brečević L. Transformation of anhydrous calcium sulphate into calcium sulphate dihydrate in aqueous solutions. J Cryst Growth 2002;240:203–11.
[29] Paul M, Glasser FP. Impact of prolonged warm (85 °C) moist cure on Portland cement paste. Cem Concr Res 2000;30:1869–77.
[30] Gu P, Beaudoin JJ, Quinn EG, Myers RE. Early strength development and hydration of ordinary Portland cement/calcium aluminate cement pastes. Adv Cem Bas Mater 1997;6:53–8.
[31] Lamberet S. Durability of ternary binders based on Portland cement, calcium aluminate cement and calcium sulfate. PhD thesis, Lausanne, Ecole Polytechnique Fédérale de Lausanne; 2005.
[32] Rettel A, Damidot D, Müller D, Gessner W. A NMR study of gels formed during the hydration of calcium aluminate cements in the presence of citrate or gluconate. In: Justnes H, editor. Proceedings 10th ICCC. Gothenburg: Amarkai AB and Congrex Göteborg AB, vol. 3 (3iii007); 1997. p. 1–8.
[33] Sugama T. Citric acid as a set retarder for calcium aluminate phosphate cements. Adv Cem Res 2006;18(2):47–57.
[34] Möschner G, Lothenbach B, Figi R, Kretzschmar R. Influence of citric acid on the hydration of Portland cement. Cem Concr Res 2009;39:275–82.
[35] Cody AM, Lee H, Cody RD, Spry PG. The effects of chemical environment on the nucleation, growth, and stability of ettringite $[Ca_3Al(OH)_6]_2(SO_4)_3·26H_2O$. Cem Concr Res 2004;34:869–81.
[36] Ito S, Suzuki K, Inagaki M, Naka S. High-pressure modifications of $CaAl_2O_4$ and $CaGa_2O_4$. Mat Res Bull 1980;15:925–32.